Chopped random-basis quantum optimization

Tommaso Caneva, Tommaso Calarco, and Simone Montangero
Institut für Quanteninformationsverarbeitung, Universität Ulm, D-89069 Ulm, Germany
(Received 22 March 2011; revised manuscript received 15 June 2011; published 22 August 2011)

In this work, we describe in detail the chopped random basis (CRAB) optimal control technique recently introduced to optimize time-dependent density matrix renormalization group simulations [P. Doria, T. Calarco, and S. Montangero, Phys. Rev. Lett. **106**, 190501 (2011)]. Here, we study the efficiency of this control technique in optimizing different quantum processes and we show that in the considered cases we obtain results equivalent to those obtained via different optimal control methods while using less resources. We propose the CRAB optimization as a general and versatile optimal control technique.

DOI: 10.1103/PhysRevA.84.022326 PACS number(s): 03.67.−a, 02.30.Yy

Realizing artificial, controllable quantum systems has represented one of the most promising challenges in physics for the past 30 years [1]. On one side, such systems could unveil unexplored features of nature, when employed as universal quantum simulators [2]; on the other side, this technology could be exploited to realize a new generation of extremely powerful devices, like quantum computers [3]. Along with the impressive progress marked recently in the construction of tunable quantum systems [4,5], there is a renewed and increasing interest in quantum optimal control (OC) theory, the study of the optimization techniques aimed at improving the outcome of a quantum process [1]. Indeed, OC can prove to be crucial under several respects for the development of quantum devices: first, it can be generally employed to speed up a quantum process to make it less prone to decoherence or noise effects induced by the unavoidable interaction with the external environment. Second, considering a realistic experimental setup in which just few parameters are tunable or, in the most difficult situations, only partially tunable, OC can provide an answer about the optimal use of the available resources.

Traditionally, OC has been exploited in atomic and molecular physics [6–8]. More recently, with the advent of quantum information, the requirement of accurate control of quantum systems has become unavoidable to build quantum information processors [9,10,12–16]. However, the above-mentioned methods often result in optimal driving fields that require a level of tunability incompatible with current experimental capabilities and, in general, the calculation of the optimal fields requires an exact description of the system (either analytical or numerical). The field of application of these methods is severely limited also by the need to have access to huge amount of information about the system, e.g., computing gradients of the control fields, expectation values of observables as a function of time. Moreover, standard OC algorithms define a set of Euler-Lagrange equations that have to be solved to find the optimal control pulse [1], where the equation for the correction to the driving field is highly dependent on the constraints imposed on the system and on the figures of merit considered. This implies that considering different figures of merit and/or constraints on the system needs a redefinition of the corresponding Euler-Lagrange equations, hindering a straightforward adaptation of the optimization procedure to different situations.

In this work, we discuss in detail the chopped random basis (CRAB) technique, an optimization method directed to overcome these difficulties and already introduced in Ref. [11]. The CRAB optimization is based on the definition of a truncated randomized basis of functions for the control fields that recast the problem from a functional minimization to a multivariable function minimization that can be performed, for example, via a direct-search method. As shown in the following, the CRAB optimization flexibility allows to construct OC pulses just exploiting the available resources. Indeed, different figures of merit and constraints can be easily considered without any complications. Another appealing characteristic of CRAB is its compatibility with time-dependent density matrix renormalization group (t-DMRG) techniques: this feature indeed significantly enlarges the class of controllable systems [11], from few-body or exactly solvable to general many-body quantum systems with "moderate" degree of entanglement generated during the dynamics [17]. This is, to the best of our knowledge, the unique OC algorithm that can be applied in such vast setting. Finally, it can be straightforward applied also in a closed-loop optimization experiment, where the simulation of the system under study is replaced with the experiments itself.

Here, we analyze the CRAB optimization as a possible general OC algorithm to be used also in a standard context (solvable and/or few body systems) as a valid alternative tool with respect to standard OC methods to find optimal control fields. Indeed, recently, optimization methods based on the expansion over a particular function basis have shown to be effective [18–21]. In particular, a similar approach has been proved to be mathematically convergent and consistent [22,23]. On top of that, some theoretical analysis over control landscapes suggests that, at least in the absence of constraints, the figure of merit landscape might be smooth enough to allow for simple optimization procedures to work [24,25]. Here, we show that a convenient choice of the function basis driven by physical or geometrical arguments is enough to obtain optimal driving fields. However, in the cases where no physical intuition drives the choice of the function basis, the CRAB algorithm allows us to find the optimal driving fields where a simple ansatz would fail. Moreover, a comparison between the results of CRAB with and without a physically driven choice of the basis, as well as previous results obtained using different optimal control algorithms (Krotov's algorithm), show comparable performances [26].

The structure of the paper is the following: in Sec. I, the CRAB optimization is described; in Sec. II, it is applied to a

paradigmatic quantum control problem, the state transformation of two coupled qubits, to show its potential. Then, we compare the results obtained via CRAB optimization in more complex cases already present in literature [26,27]: in Sec. III, the method is employed to control the quantum phase transition evolution of the Lipkin-Meshkov-Glick (LMG) model; and in Sec. IV, we optimize the transfer of a state along a spin chain. Finally, in Sec. V, the optimization is exploited to maximize the final entanglement entropy of the final state in the LMG model; and in Sec. VI, a comparison between adiabatic and optimized processes is proposed.

I. CRAB OPTIMIZATION

The optimization problem we are dealing with is defined as follows: given a Hamiltonian H acting on a Hilbert space $\mathcal{H} = \mathbb{C}^N$, depending on a set of time-dependent driving fields $\vec{\Gamma}(t)$, we search for the optimal transformation to drive, in time T, an initial state $|\psi_0\rangle \in \mathcal{H}$ into a different one (target state) $|\psi_G\rangle \in \mathcal{H}$ with some desired properties expressed by a cost function $f(|\psi_G\rangle)$ we want to minimize.[1] In addition, constraints might be present on the driving fields, e.g., to match experimental conditions: they can be expressed usually as a function of the driving fields $\mathcal{C}_i[\vec{\Gamma}(t)]$. Typical scenarios and corresponding cost functions and constraints are:

(1) The goal is the preparation of a well-defined quantum state $|\psi_G\rangle$ with high accuracy for which a convenient cost function is the infidelity,

$$f_1[|\psi(T)\rangle] \equiv \mathcal{I}(T) = 1 - |\langle\psi(T)|\psi_G\rangle|^2. \tag{1}$$

(2) The target state is the unknown ground state of a Hamiltonian H_p. The cost function is then given by the final system energy,

$$f_2[|\psi(T)\rangle] \equiv E_f(T) = \langle\psi(T)|H_p|\psi(T)\rangle. \tag{2}$$

(3) The target is some property or condition that many states can satisfy, like, for example, in the production of highly entangled states. In this case, the cost function is simply defined as

$$f_3[|\psi(T)\rangle] \equiv -S[|\psi(T)\rangle], \tag{3}$$

where $S[|\psi\rangle]$ is a convenient measure of the entanglement of the state $|\psi\rangle$.

(4) A constraint is present on the power of the driving fields, that is, the solution should minimize also the fluences

$$\mathcal{C}_i = \int |\Gamma_i(t)|^2 dt. \tag{4}$$

(5) A limited bandwidth is allowed for the driving fields: below we show how this is already embedded in the algorithm and is not necessary to consider it as an additional explicit constraint.

(6) The initial state or the driving fields are known within a given uncertainty ϵ. In this case, the cost function can be defined as an average of all other possible outcomes compatible with that uncertainty, as for example,

$$f_4 = \int f[|\psi(T,\epsilon)\rangle] d\epsilon. \tag{5}$$

All of the aforementioned optimization problems are then recast in the problem of solving the Schödinger equation (from now on we assume $\hbar = 1$),

$$i\frac{d}{dt}|\psi(t)\rangle = H[\vec{\Gamma}(t)]|\psi(t)\rangle, \tag{6}$$

with boundary condition $|\psi_i\rangle = |\psi(0)\rangle$, while minimizing the cost function

$$\mathcal{F} = \alpha f + \sum_i \beta_i \mathcal{C}_i[\Gamma(t)], \tag{7}$$

where the coefficients α and β_i allow for a proper weighting of the different contributions (the βs play the role of Lagrange multipliers) and f is the chosen cost function.

To perform such an optimization, the CRAB algorithm starts from an initial pulse guess $\Gamma_j^0(t)$ and then looks for the best correction of the form

$$\Gamma_j^{\mathrm{CRAB}}(t) = \Gamma_j^0(t) g_j(t). \tag{8}$$

The functions $g_j(t)$ are expanded in a simple form in some function basis characterized by some parameters $\vec{\Omega}_j$ (Fourier space, Lagrange polynomials, etc.): $g_j = \sum_k c_j^k \hat{g}_j^k(\Omega_j^k)$. The two key ingredients of the CRAB optimization are that the function space is truncated to some finite number of components N_c ($k = 1, \ldots, N_c$) and that the corresponding basis functions are "randomized" to enhance the algorithm convergence, i.e., $\hat{g}_j^k \to \hat{g}_j^k[\Omega_j^k(1 + r_j^k)]$, where r_j^k is a random number. Indeed, this last choice breaks the orthonormalization of the functions g_j^k; however, as we show in the following, it allows for an improved convergence of the algorithm as it enlarge the subspace of functions explored by the algorithm while keeping constant the number of optimization parameters.

The optimization problem is then reformulated as the extremization of the multivariable cost function $\mathcal{F}(T, \vec{c}_j)$, which can be numerically approached with a suitable method, e.g., steepest descent, conjugate gradient, or direct search methods [28]. Hereafter, we use the last option, which is the simplest one and easily compatible with any technique employed to solve the dynamics induced by $H[\Gamma(t)]$ (either exact solution of the Eq. (6) or approximate solution with time dependent DMRG [17]). This choice also gives another advantage with respect to other OC methods where gradients and functional derivatives have to be computed, increasing the complexity of the optimization procedure.

As an example, in the following problems, we focus on the case of a single control parameter $\Gamma(t)$ and we choose to work in the Fourier basis. The optimal pulse can then be written as

$$g(t) = 1 + \frac{\left[\sum_{n=1}^{N_c} A_n \sin(\omega_n t) + B_n \cos(\omega_n t)\right]}{\lambda(t)}, \tag{9}$$

where $\lambda(t)$ is a time dependent function enforcing the boundary conditions [i.e., $\lambda(t) \to \infty$ for $t \to 0$ and for $t \to T$]. The function $\Gamma^{\mathrm{CRAB}}(t)$ is fixed by selecting the optimization parameters $\vec{A}, \vec{B}$, and $\vec{\omega}$, with N_c the dimension of each vector.

[1] The generalization of the problem to the optimization of an overall unitary transformation is straightforward, averaging over the contributions of a complete set of basis of the Hilbert space $\mathcal{H}$.

In conclusion, given a fixed total evolution time T, the cost function is clearly just a function of the control parameters,

$$\mathcal{F} = \mathcal{F}^{\mathrm{CRAB}}(\vec{A},\vec{B},\vec{\omega}). \tag{10}$$

The optimization problem is reduced to the minimization of $\mathcal{F}^{\mathrm{CRAB}}(\vec{A},\vec{B},\vec{\omega})$ as a function of $3\times N_c$ variables. As mentioned before, however, the space of the variables can be reduced even more: although in principle the frequencies $\vec{\omega}$ can be considered free variables, it is often convenient to keep them fixed and to perform the minimization just with respect to $\vec{A}$ and $\vec{B}$. Indeed, as shown in our analysis, this is sufficient to obtain good results. In this approach we need then a criterion to select the $\vec{\omega}$'s. When we have no available information about the typical energy scales of the system under consideration, the frequencies are picked *randomly* around principal harmonics: $\omega_k = 2\pi k(1+r_k)/T$, with r_k random numbers with flat distribution in the interval $[-0.5,0.5]$ and $k = 1,\ldots,N_c$. Vice versa when the physical details of the model are known, clearly one can exploit this information to select the relevant frequencies, as shown in the following sections.

II. TWO-QUBIT OPTIMIZATION

In this section, we apply the CRAB optimization to a paradigmatic problem in quantum information theory and control: we search for the optimal way to perform a state transformation of a two-qubit system; in particular, we consider two capacitively coupled Josephson charge qubits, even though the following analysis can be easily adapted to different qubit implementations. The Hamiltonian of the i-th qubit is defined as [29,30]

$$\mathcal{H}_i = E_C\sigma_z^i + E_J\sigma_x^i,$$

where the σs are Pauli matrices, E_C is the charging energy, E_J is the Josephson energy, and $i = 1,2$. For capacitive coupled qubits, the interaction Hamiltonian reads

$$\mathcal{H}_I = E_{cc}\sigma_z^1\sigma_z^2,$$

where E_{cc} is the charging energy associated to the Coulomb interaction between the qubits. Hereafter we set $E_J/E_C = -1$, while the coupling will be the driving field $E_{cc}(t)/E_C = \Gamma(t)$ we use to optimize the transformation. We will consider as initial state the state with no excess Cooper pairs $|\psi_0\rangle = |00\rangle$, and our goal states will be three different states with different properties: the reversed separable state $|\psi_G^1\rangle = |11\rangle$, the homogeneous superposition state $|\psi_G^2\rangle = \frac{1}{2}\sum_{i,j}|i,j\rangle$, and the maximally entangled Bell state $|\psi_G^3\rangle = \frac{1}{\sqrt{2}}(|00\rangle + |11\rangle)$. Note that due to the fact that only the coupling is controlled, all three states are not trivial to achieve. We set the total time of the transformation to the somehow arbitrary time scale $T = \pi/E_J$ and we perform a CRAB optimization using the truncated expansion of the function $g(t)$ given in Eq. (9), with a constant initial guess for the driving field $\Gamma^0(t) = \Gamma(0) = 1$. We considered an additional constraint on the fluence of the control field, thus the resulting cost function is defined as

$$\mathcal{F} = f_1 + 0.1\,\mathcal{C}_1[\Gamma(t)], \tag{11}$$

where f_1 and $\mathcal{C}_1$ are given by Eqs. (1) and (4), respectively. Here we are interested in studying the effect of the randomness introduced in the frequencies of the expansion Eq. (9), thus we optimize both in the case of random r_k and with $r_k = 0$. To perform a fair comparison, we ran the optimization in both cases with the same maximum number of calls $N_f \sim 30.000$ to the function $\mathcal{F}$, which fixes the simulation complexity. Indeed, in the first case we repeated the optimization for 30 different r_k random configurations (with a single A_k, B_k random starting point), while in the second case the optimization was repeated over 30 initial random A_k, B_k configurations. A typical result is shown in Fig. 1 for $N_c = 2$ and $|\psi_G^1\rangle$: it clearly shows that for the case of randomized ω_k the optimization is highly improved (notice the logarithmic scale). A more systematic comparison is shown in Fig. 2, where the best results are plotted against the number of optimization parameters N_c for the three target states $|\psi_G^i\rangle$: in all cases the randomization of the frequencies improves the convergences to higher fidelities up to the simulation error. In particular, in one case, the final result without randomization is very far from being satisfactory as the final fidelity is of the order of ten percent, resulting in a very poor state transformation. On the contrary, using the randomized frequencies we were able to find optimal pulses to obtain fidelities below one percent—values that are comparable, in most cases, with experimental errors.

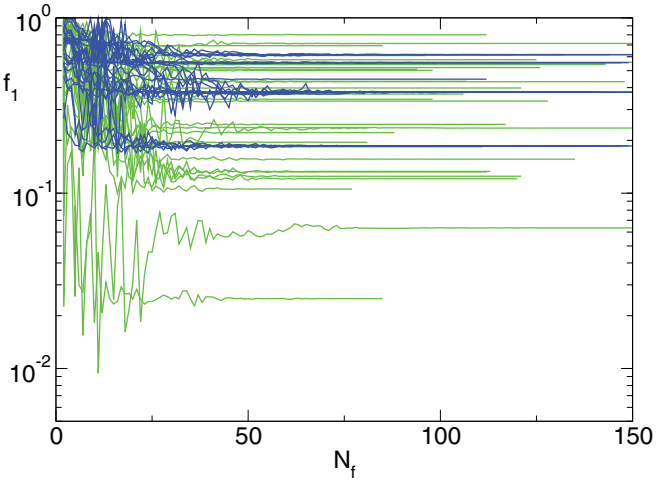

FIG. 1. (Color online) Infidelity f_1 of the final state as a function of number of calls to the optimization algorithm N_f for two capacitively Josephson charge qubits with principal harmonics [dark grey (blue) line] and randomized frequencies [light grey (green) line], for the goal state $|\psi_G^1\rangle$ and $N_c = 2$ for 30 different random instances.

III. LIPKIN-MESHKOV-GLICK MODEL

The Lipkin-Meshkov-Glick (LMG) model is the paradigm of a system with long-range interaction (infinite in the thermodynamical limit). The Hamiltonian is written as [31,32]:

$$H = -\frac{J}{N}\sum_{i<j}\left(\sigma_i^x\sigma_j^x + \gamma\sigma_i^y\sigma_j^y\right) - \Gamma(t)\sum_i^N\sigma_i^z, \tag{12}$$

where J is the uniform spin-spin interaction (we set $J = 1$ in the following), N is the number of spins in the system, Γ is the transverse field, and σ_i^α are the Pauli matrices. By introducing the total spin operator $\mathcal{S}_\alpha = \sum_i \sigma_i^\alpha/2$, Eq. (12) can be rewritten, apart from an additive constant, as

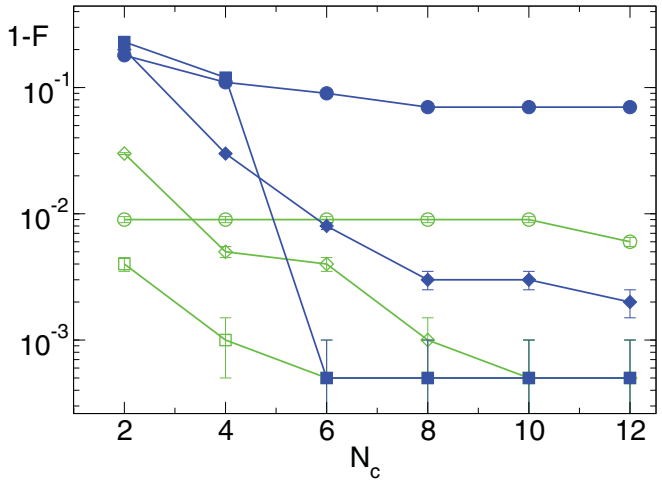

FIG. 2. (Color online) Optimized infidelity f as a function of the number of optimization parameters N_c with principal harmonics [dark grey (blue), full symbols] and randomized frequencies [light grey (green), empty symbols] for different target states $|\psi_G^1\rangle$ (circle), $|\psi_G^2\rangle$ (squares), $|\psi_G^3\rangle$ (diamonds).

$H = -\frac{1}{N}[\mathcal{S}_x^2 + \gamma\mathcal{S}_y^2] - \Gamma\mathcal{S}_z$. The Hamiltonian hence commutes with $\mathcal{S}^2$ and does not couple states having a different parity in the number of spins pointing in the magnetic field direction: $[H,\mathcal{S}^2] = 0$ and $[H, \prod_i \sigma_i^z] = 0$. In the isotropic case $\gamma = 1$, also the z component of $\vec{\mathcal{S}}$ is conserved, $[H,\mathcal{S}_z] = 0$. In the thermodynamical limit, the LMG model undergoes a second-order quantum phase transition at $\Gamma_c = 1$ from a paramagnet ($\Gamma > 1$) to a ferromagnet ($\Gamma < 1$). The phase transition is characterized by mean-field critical exponents [32]. The phase transitions dramatically affects the dynamical behavior of quantum systems: as discussed in more detail in Sec. VI, the gap closure at the critical point promotes dynamical excitations, preventing adiabatic evolutions whenever the adiabaticity condition $T \gg \Delta^{-1}$ is not fulfilled, where T is the total evolution time and Δ the minimum spectral gap [33–42]. Following Ref. [26], we employ the CRAB optimization to drastically reduce the residual density of defects present in the system in a strongly nonadiabatic dynamics, drastically reducing the time needed to connect the ground state in one phase with the ground state of the other phase with respect to adiabatic nonoptimized strategies. We chose as initial state the ground state (gs) of $H[\Gamma(t)]$ at $\Gamma_i \gg 1$, i.e., the state in which all the spins are polarized along the positive z axis (paramagnetic phase). As target state, we chose the gs of $H[\Gamma = 0]$ (ferromagnetic phase). We focused our attention on the case $\gamma = 0$, representative of the class $\gamma < 1$ (for $\gamma = 1$ the dynamics is trivial due to the symmetry of H) [43]. For this model, indeed, a lot of physical information is available: the gap between the ground state and the first excited state closes polynomially with the size at the critical point [32], $\Delta \sim N^{-1/3}$. Furthermore, it has been recently demonstrated that the minimum time required to obtain a perfect conversion between the initial and the final state here considered, the so called *quantum speed limit*, is given by $T_{\rm QSL} = \pi/\Delta$ [26,44]. In order to test the performance of CRAB, we fixed the total evolution time above this threshold, at $T = 2T_{\rm QSL}$, in a regime

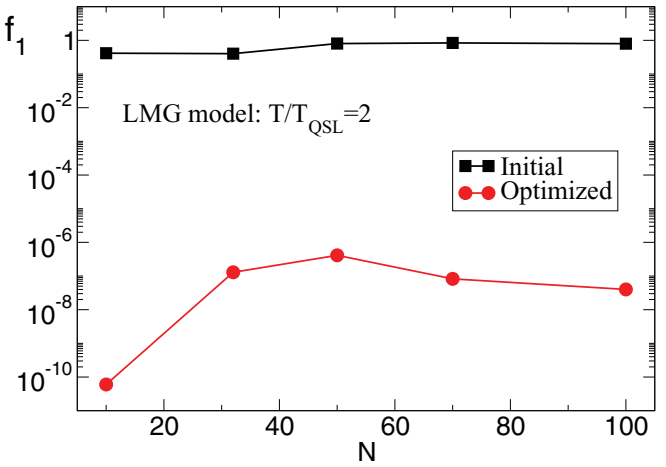

FIG. 3. (Color online) Infidelity as a function of the size in the LMG model. Squares represent the data before the optimization; circles the data after the optimization with CRAB.

in which in principle it is possible to produce an arbitrarily small infidelity with optimized evolutions.

The results of our simulations for the LMG model are summarized in Figs. 3 and 4; the data shown in the two pictures (with the only exception of the inset of Fig. 4 as explained in the following) have been produced assuming Eq. (9) as control field and the infidelity as cost function to minimize. In Fig. 3, we plotted the infidelity as a function of the size N, before the optimization for a linear driving field $\Gamma^0(t) \propto t/T$ (squares), and after the optimization with CRAB (circles): for each size we have been able to produce an infidelity below 10^{-6} starting from an infidelity of order $O(1)$. In particular, the data have been produced by minimizing Eq. (10) with respect to $\vec{A}$ and $\vec{B}$, while keeping $\vec{\omega}$ fixed, for a total of $2 \times N_c = 16$ parameters. In this case, the frequencies $\vec{\omega}$ have been chosen by exploiting the physical information available.

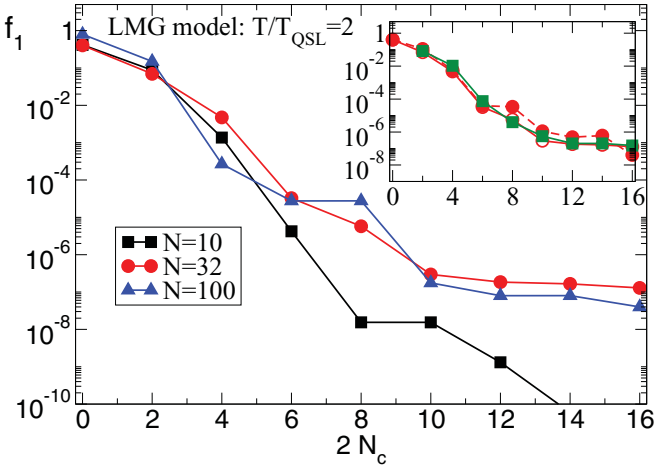

FIG. 4. (Color online) Infidelity as a function of the number of control parameters for different sizes in the LMG model. The total evolution time is $T = 2T_{\rm QSL} = 2\pi/\Delta$. Inset: infidelity as a function of the number of parameters for a single size $N = 32$: comparison between data optimized using as cost function the infidelity (empty circles) and the final energy (full circles). Green squares represent the results with randomized frequencies.

We chose the frequencies equal to the minimum spectral gap $\omega_1 = 2\pi/T = 2\pi/2T_{\rm QSL} = \Delta$ and we considered the main harmonics $\omega_k = k\omega_1$ for k up to N_c. In Fig. 4, we plot the infidelity as a function of number of parameters employed to build the optimal field of Eq. (9)—adding a frequency ω_k corresponds to add two parameters, A_k and B_k. First, it can be noticed that 5 harmonics are sufficient to reach the best optimization result, $\mathcal{I} \sim 10^{-6}$; however, with only 3 harmonics the infidelity is already of order 10^{-4}, of the order of the required threshold for fault-tolerant quantum computation. Considering the implementation of an optimal pulse in an NMR or quantum optics experiment, the gain with respect to other OC methods providing a totally arbitrary $\Gamma_{\rm opt}(t)$ is evident. The second interesting feature is that the behavior of the infidelity in Fig. 4 is approximately independent of the size (for the smallest system considered, $N = 10$, finite size effects are more evident): this confirms the intuition that the most relevant energy scale for the LMG model is given by the minimum spectral gap.

Finally, in order to verify the independence of the optimization from the knowledge of the target state, we repeated the simulations assuming as a cost function the final energy $E_f(T)$ of Eq. (2). In the inset of Fig. 4, we compare the infidelity of the data optimized using as cost function the infidelity itself (empty circles) and the final energy (full circles), for a specific size of the system $N = 32$ and for different number of control parameters: as shown in the picture, the agreement is very good. We also repeated the optimization using randomized frequencies, obtaining the same results as before. Thus, also in the case where the chosen frequencies are optimal, introducing randomness does not prevent the optimization to work. On the contrary, if one has no access to any information on the system, the randomization does not prevent reaching the same optimal result.

IV. STATE TRANSFER ALONG A SPIN CHAIN

In this section, we study the optimization of a model representing a possible implementation of a quantum bus. The model consists in a chain of spins coupled via uniform nearest-neighbor (n.n.) interaction; by acting with an external, parabolic magnetic field, it is possible to transfer a quantum state along the chain [9,27,45]. In particular, we follow the lines of Refs. [45,46]. The Hamiltonian of the system is

$$H(t) = -\frac{J}{2}\sum_{n=1}^{N-1}\vec{\sigma}_n \cdot \vec{\sigma}_{n+1} + \sum_{n=1}^{N} B_n(t)\sigma_n^z, \qquad (13)$$

where N is the number of spins in the chain, $\vec{\sigma}_n$ represents the Pauli n-th-spin operator, J is the uniform n.n. interaction (we set $J = 1$ in our simulations), and $B_n(t)$ is the tunable magnetic field along the z direction. In particular, we considered a parabolic magnetic field tunable in position and strength [45],

$$B_n(t) = C(t)[x_n - d(t)]^2, \qquad (14)$$

where $d(t)$ is the position of the potential minimum along the chain, x_n is the position of the n-th spin, and $C(t)$ is the instantaneous curvature of the field. Far from the minimum, the spins are forced by the magnetic field to be aligned along the z axis irrespective of their mutual interaction; instead close to the minimum, the n.n. coupling prevails and can be exploited to transfer the information (i.e., the state) from one site to the next. The Hamiltonian commutes with the total magnetic field along the z direction, $[H(t), \sum_{n=1}^{N}\sigma_n^z] = 0$, so that the dynamics occurs in a subspace whose dimension grows just linearly with the size N of the system. We chose to work in the subspace $\langle\sum_{n=1}^{N}\sigma_n^z\rangle = 1$; in particular, we aimed at transferring a spin-up state from one end of the chain to the opposite end, or in other words to transform the state $|\psi_i\rangle = |10...0\rangle$ into the state $|\psi_G\rangle = |0...01\rangle$, with 0 (1) corresponding to the n-th spin pointing in the down (up) direction along the z axis. We employed CRAB to optimize the two control parameters, $\Gamma_1(t) = d(t)$ and $\Gamma_2(t) = C(t)$; as in the previous section, we set the total evolution time above the quantum speed limit threshold at the value $T = 2T_{\rm QSL}$, where for the latter we used the estimate made in Refs. [27,45]. The optimization has been performed by keeping $\vec{\omega}_1, \vec{\omega}_2$ fixed (in particular $\omega_{1k} = \omega_{2k} = 2k\pi/T$ for $k = 1,...,N_c$) and minimizing the infidelity with respect to $\vec{A}_1, \vec{B}_1, \vec{A}_2, \vec{B}_2$, where the index 1 and 2 refer to $d(t)$ and $C(t)$, respectively.

The results of our simulations for the state transfer along the chain are summarized in Figs. 5 and 6. In Fig. 5, we show the infidelity as a function of the size before the optimization (squares), for a constant $C(t)$ and $d(t) = t/T$, and after the optimization with CRAB (circles): for each size considered, we were able to reach an infidelity below the value 10^{-4} starting from an initial infidelity of order 1. In Fig. 6, we plot the infidelity as a function of the number of parameters employed in the minimization procedure; in this case, unlike for the LMG model in Fig. 4, the data show a strong dependence on the size. We interpreted this behavior as a consequence of the structure of the problem. Considering the particular transfer mechanism, in which the information moves step by step from one site to the next one, we expect the optimal pulse to be able to modulate the magnetic field around each spin; this occurs only when the spectrum of the pulse involves frequencies of the order of the inverse of the time spent on a generic site n; i.e., $\omega \sim 2\pi/(T/N) = N\omega_1$. As a test, in the inset of Fig 4 we plotted the infidelity as a function of the number of parameters

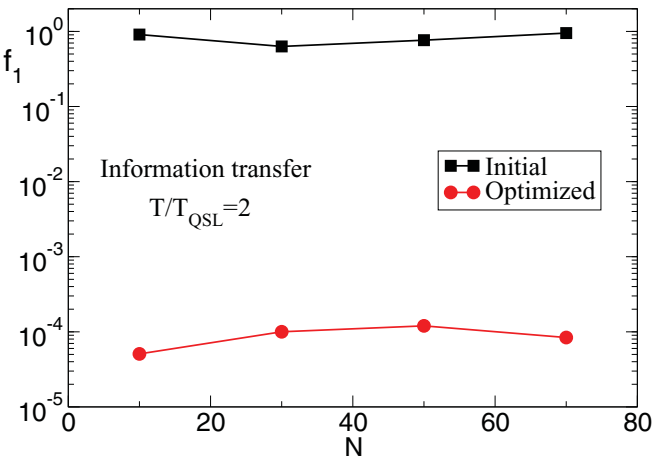

FIG. 5. (Color online) Infidelity as a function of the size in the transfer state problem. Squares represent the data before the optimization; circles the data after the optimization with CRAB.

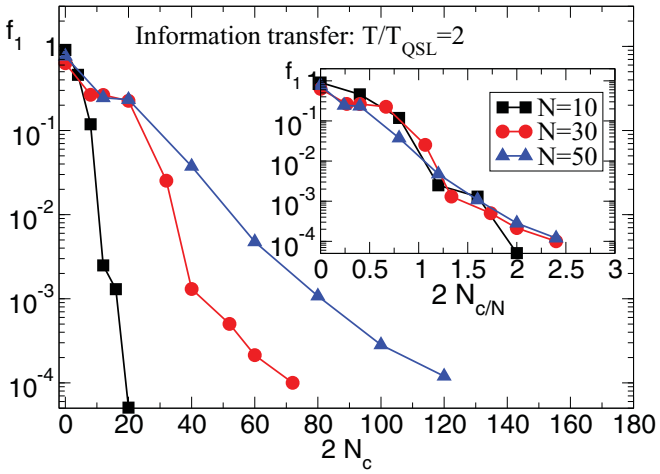

FIG. 6. (Color online) Infidelity as a function of the number of control parameters for different sizes in the in the state transfer model. The total evolution time $T = 2T_{\mathrm{QSL}}$. Inset: infidelity as a function of the number of parameters divided by the size.

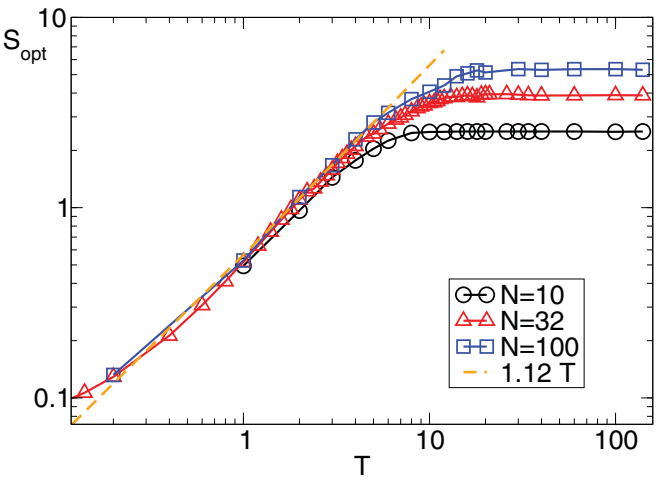

FIG. 7. (Color online) Final entanglement entropy as a function of the total evolution time T for $N = 10,32$, and 100 of one of two equal bipartitions of the system. The time is measured in units of J^{-1}.

divided by the size; the good agreement of the rescaled data confirms our expectation.

V. ENTANGLEMENT ENTROPY MAXIMIZATION

Among its various applications, OC can be exploited for entanglement production [47,48]. Here we employ the CRAB technique in the LMG model to maximize the von Neumann entropy $S_{L,N} = -\mathrm{Tr}(\rho_{L,N} \log_2 \rho_{L,N})$ associated to the reduced density matrix $\rho_{L,N}$ of a block of L spins out of the total number N at a given final time T, which gives a measure of the entanglement present between two bipartitions of a quantum system. As seen in Sec. III, due to the symmetry of the Hamiltonian $[H,\mathcal{S}^2] = 0$, the dynamics is restricted to subspaces with fixed total angular momentum; in particular, assuming as initial state the ground state of the system, we have $\mathcal{S} = N/2$. The Dicke states $|\mathcal{S} = N/2,\mathcal{S}^z\rangle$ with $\mathcal{S}^z = -N/2,...,N/2$ provide a convenient basis spanning the subspace accessible through the dynamics. Indeed the entanglement entropy $S_{L,N}$ can be easily evaluated noticing that, since the maximum value of the total spin can be achieved only with maximum value of the spin in each bipartition, the following decomposition holds [43,49]:

$$|N/2,n\rangle = \sum_{l=0}^{L} p_{l,n}^{1/2} |L/2,l - L/2\rangle \otimes |(N-L)/2,n-l-(N-L)/2\rangle, \quad (15)$$

where n and l correspond, respectively, to the number of up spins in the whole system and in the block of size L, and $p_{l,n} = L!(N-L)!n!(N-n)!/[l!(L-l)!(n-l)!(N_L - n+l)!N!]$. Expressing the evolved state $|\psi(T)\rangle$ in the Dicke state basis and using the previous decomposition, it is immediate to evaluate $S_{L,N}(T)$.

In our simulations, we considered a system equally bipartite, i.e., $L = N/2$, and we took as starting state the ground state of the LMG Hamiltonian at $\Gamma \gg 1$, in which all the spins are polarized along the positive z direction, so that the state factorizes and the entanglement entropy vanishes; see Fig. 7.

Then we performed the optimization with CRAB, modulating the field according to Eq. (9) and using as a cost function Eq. (3). The behavior of entanglement entropy after the optimization $S_{\mathrm{opt}}(T)$ for different values of the total evolution time T is shown in Fig. 7: after a short transient of linear growth, $S_{\mathrm{opt}}(T)$ reaches a saturation value growing with the size, as expected. It is interesting to notice that such a behavior closely resembles the features observed in one-dimensional systems after a sudden quench [50], although here we are dealing with a fully connected model [51,52]. In Fig. 8, we plotted the saturation value reached with the optimization as a function of the size N; comparing our data with the maximum possible value of the von Neumann entropy for a subsystem of $L = N/2$ spins (described by a Hilbert space of dimension $N/2+1$) $S_{\mathrm{max}} = \log_2(N/2+1)$, we obtain almost the maximal possible amount of entanglement, $S_{\mathrm{opt}}/S_{\mathrm{max}} \sim 0.95$.

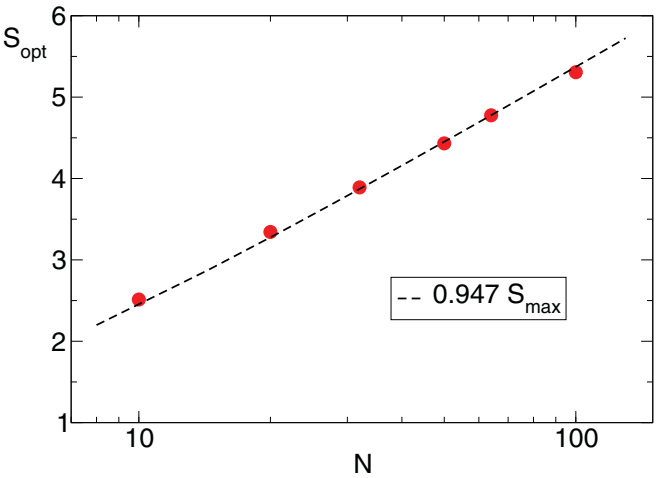

FIG. 8. (Color online) Entanglement entropy saturation value as a function of the size (red circles) and the function $A \log_2(N/2+1)$ (dashed line). A fit gives $A = 0.947$.

VI. LINEAR VS. OPTIMAL DRIVING

In this section, we analyze in more detail the features characterizing the optimal dynamics induced by CRAB. In order to better understand the matter, we draw a comparison with a simpler nonoptimized dynamics, in which the driving field is linearly dependent on time; in particular, we focus the attention on the LMG model. An important point in the study of the dynamics of a quantum system is usually represented by the *adiabatic theorem* [33]. The latter establishes that a system initially prepared in its ground state can be driven by a time-dependent Hamiltonian adiabatically (i.e., without introducing excitations), if the time scale of the evolution is much larger than the minimum spectral gap; i.e., $T \gg \Delta^{-1}$. In critical systems, the spectral gap closes at the phase transition, so that the system gets excited from the instantaneous gs while crossing the critical point for any finite-time evolution [34]. For finite-size systems, the critical gap is not completely closed, but it presents a pronounced minimum where the excitation appears, as shown in Fig. 9: an estimate of the excitations induced by a linear driving can be obtained by Kibble-Zurek theory [35,37,41,43,53]. In Fig. 9, we monitored the instantaneous total excitation probability $P_{\rm tot}$ (dashed line) and the populations of lowest levels [different style (color) lines] during the dynamics. The evolution starts at large negative times (left) and ends at the time $t = 0$ (right); the critical point is crossed around the time $t = 11$ when $\Gamma(t) \sim 1$; see Sec. III. Far from the critical point, the system evolves adiabatically as demonstrated by the low total instantaneous excitation probability; notice that before reaching the critical point, the total excitation probability coincides with the small excitation of only the first level (red continuous line). In a restricted region around the critical point ($-15 < t < -10$), the total excitation probability jumps to values of order 1

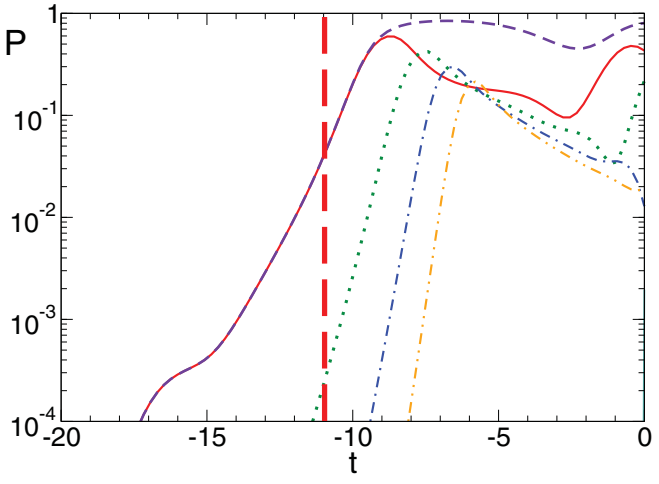

FIG. 9. (Color online) Instantaneous excitation probabilities P_i of the i-th excited level (P_1, continuous; P_2, dotted; P_3, dot-dashed; P_4, dot-dot-dashed; P_{25}, dash-dash-dotted line) and total excitation probability $P_{\rm tot} = \sum_{i=1}^{N} P_i$ (dashed purple line) in the LMG model with $N = 50$ for an evolution induced with a driving field linear in time, $\Gamma(t) \propto -t/T$, $T/T_{\rm QSL} = 2$, $N = 50$. The thick (red) dashed line signals the crossing of the critical point. The time is measured in units of J^{-1}.

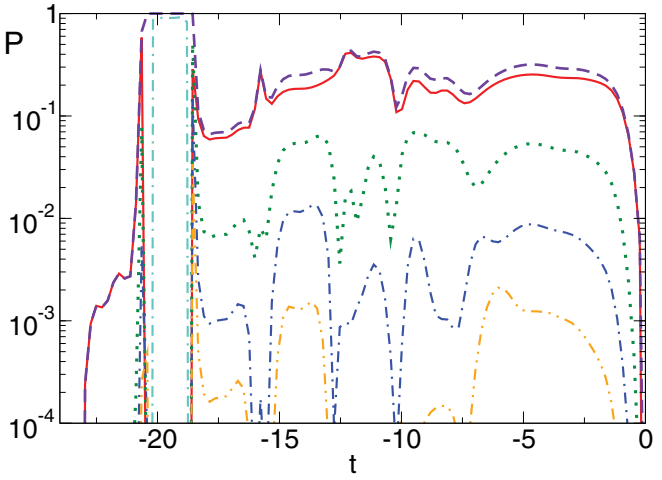

FIG. 10. (Color online) Optimal instantaneous excitation probabilities P_i in the LMG model for $T/T_{\rm QSL} = 2$, $N = 50$. Codes are the same as described in the legend of Fig. 9. The time is measured in units of J^{-1}.

and does not change significantly any more. Notice that in the final part of the evolution, more levels get populated, as shown by the difference between the instantaneous infidelity and the excitation probability of the first level. At the final time $t = T$, the excitation probability is equal to the infidelity of the process; i.e., $P_{\rm tot}(T) = f_1$. We then optimize the final infidelity, and the correspondent plot for the optimal evolution is reported in Fig. 10. The scenario in this case is completely different: the system is excited at the very beginning of the dynamics and remains excited for the most part of the evolution until close to the end, when the infidelity drops abruptly to zero. It is interesting to notice that just a few levels are excited, as demonstrated by the small difference between the total excitation probability (dashed line) and the excitation probability of the first level (red continuous line). This result is in agreement with previous findings where the authors showed that this kind of dynamics can be approximated by a two-level system dynamics [26]. The abrupt jump in the probabilities around time 20 is due to an abrupt (double) change of sign in $\Gamma_{\rm CRAB}(t)$, reversing suddenly the order of the levels and transforming the gs in the most excited state [dash-dash-dotted (cyan) line]; thus, this signature is not due to a collective involvement of all the levels but simply to a reshuffling of their order. Indeed, as shown in the picture for $-18 < t < 0$, with the subsequent change of sign the previous order is reestablished. We can then summarize the main features of the optimal evolution induced by CRAB in three points: it is strongly nonadiabatic, it involves just a restricted number of levels although not necessarily close to the nominal instantaneous ground state, and it is such that at the very end all populations constructively interfere to obtain the desired goal state.

VII. CONCLUSIONS

In this paper, we studied in detail the performance of quantum optimal control through the CRAB optimization [11]. In particular, we focused our attention on three different

systems and different figures of merit, in order to outline the versatility of the method. We first studied the optimization of state transformations of two qubits via a controlled coupling. We have shown that the CRAB optimization is very effective already using only a few optimization parameters and the fundamental role that the randomization of the function basis plays in increasing the process convergence. We then analyzed two many-body quantum systems: the first one, the LMG model, is the prototype of many-body systems with long-range interaction undergoing a quantum phase transition. The success of CRAB in this context confirms the possibility of controlling complex systems typically studied in condensed-matter physics, with relatively small resources: due to the unique features of CRAB, only a few parameters (three frequencies) are indeed sufficient to obtain excellent results. The second many-body quantum system studied, the transfer of information along a spin chain, is a typical problem studied in quantum information theory: the high accuracy achievable through CRAB optimization makes it a valuable tool for this kind of application. Moreover, due to the simple structure of the optimal pulses, they may be used to extract information on the typical timescales involved on the system dynamics, as we did for the information transfer in spin chains. We stress also that the exponential dependence of the figures of merit as a function of the number of parameters found in all cases (see Figs. 2, 4, and 6) suggests that, in general, a moderate number of optimization parameters will be sufficient to get huge improvements in the desired processes.

Finally, we have shown that with a simple change of the cost function, the CRAB optimization can be used to optimize the search of the unknown ground state of a Hamiltonian or to generate quantum states satisfying desired properties, i.e., high entangled states. Monitoring the instantaneous excitation probabilities generated by the optimized process, we have demonstrated the highly nonadiabatic character of the dynamics and the fact that, despite the complexity of the system under study, just a restricted number of excited levels are really populated during the evolution. The latter fact justifies the compatibility of CRAB with DMRG-like techniques. We mention that the CRAB optimization has been applied also to open quantum systems obtaining interesting results and thus increasing its possible applications [54].

In conclusion, the main features of the CRAB optimization—versatility (different constraints, compatibility with approximate simulation methods and experiments), fast convergence (the final error scales exponentially with the number of optimization parameters while the number of algorithm iterations linearly), and simplicity (small modification to existing numerical codes for quantum system simulations)—demonstrate that the CRAB optimization is not only an unique solution for many-body quantum systems optimal control but it is a valid alternative also in many different settings where other optimal control tools exist [1].

ACKNOWLEDGMENTS

We acknowledge discussions with R. Fazio, V. Giovannetti, M. Murphy, and G. Santoro, and support from the EU projects AQUTE, PICC, the SFB/TRR21, and the BWgrid for computational resources.

[1] C. Brif, R. Chakrabarti, and H. Rabitz, New J. Phys. **12**, 075008 (2010).
[2] R. Feynman, Int. J. Theor. Phys. **21**, 467 (1982).
[3] S. Lloyd, Nature (London) **406**, 1047 (2000).
[4] I. Bloch, J. Dalibard, and W. Zwerger, Rev. Mod. Phys. **80**, 885 (2008).
[5] G. Roati, C. D'Errico, L. Fallani, M. Fattori, C. Fort, M. Zaccanti, G. Modugno, M. Modugno, and M. Inguscio, Nature (London) **453**, 895 (2008).
[6] A. P. Peirce, M. A. Dahleh, and H. Rabitz, Phys. Rev. A **37**, 4950 (1988).
[7] T. Calarco, U. Dorner, P. Julienne, C. J. Williams, and P. Zoller, Phys. Rev. A **70**, 012306 (2004).
[8] N. Khaneja, T. Reiss, C. Kehlet, T. Schulte-Herbruggen, and S. G. Glaser, J. Magn. Reson. **172**, 296 (2005).
[9] S. Bose, Phys. Rev. Lett. **91**, 207901 (2003).
[10] S. Montangero, T. Calarco, and R. Fazio, Phys. Rev. Lett. **99**, 170501 (2007).
[11] P. Doria, T. Calarco, and S. Montangero, Phys. Rev. Lett. **106**, 190501 (2011).
[12] V. F. Krotov, *Global Methods in Optimal Control Theory* (Marcel Dekker, New York, 1996).
[13] A. Carlini, A. Hosoya, T. Koike, and Y. Okudaira, Phys. Rev. Lett. **96**, 060503 (2006).
[14] A. T. Rezakhani, W.-J. Kuo, A. Hamma, D. A. Lidar, and P. Zanardi, Phys. Rev. Lett. **103**, 080502 (2009).
[15] F. Verstraete, M. M. Wolf, and J. I. Cirac, Nat. Phys. **5**, 633 (2009).
[16] A. Spörl, T. Schulte-Herbrüggen, S. J. Glaser, V. Bergholm, M. J. Storcz, J. Ferber, and F. K. Wilhelm, Phys. Rev. A **75**, 012302 (2007).
[17] U. Schollwöck, Rev. Mod. Phys. **77**, 259 (2005).
[18] O. Romero Isart and J. J. Garcia-Ripoll, Phys. Rev. A **76**, 052304 (2007).
[19] L. Jiang, A. M. Rey, O. Romero Isart, J. J. Garcia-Ripoll, A. Sanpera, and M. D. Lukin, Phys. Rev. A **79**, 022309 (2009).
[20] F. Galve, D. Zueco, G. Reuther, and S. Kohler, Eur. Phys. J. Special Topics **180**, 237 (2010).
[21] C. DiFranco, M. Paternostro, and M. S. Kim, Phys. Rev. A **81**, 022319 (2010).
[22] J.-S. Li, J. Ruths, and D. Stefanatos, J. Chem. Phys. **131**, 164110 (2009).
[23] J. Ruths and J.-S. Li (2011), e-print arXiv:1102.3713.
[24] H. Rabitz, M. Hsieh, and C. Rosenthal, Science **303**, 1998 (2004).
[25] H. Rabitz, T. S. Ho, M. Hsieh, R. Kosut, and M. Demiralp, Phys. Rev. A **74**, 012721 (2006).
[26] T. Caneva, T. Calarco, R. Fazio, G. E. Santoro, and S. Montangero Phys. Rev. A **84**, 012312 (2011).
[27] T. Caneva, M. Murphy, T. Calarco, R. Fazio, S. Montangero, V. Giovannetti, and G. E. Santoro, Phys. Rev. Lett. **103**, 240501 (2009).

[28] W. H. Press, S. A. Teukolsky, W. T. Vetterling, and B. P. Flannery, *Numerical Recipes in C: The Art of Scientific Computing* (Cambridge University Press, Cambridge, 1992), 2nd ed.
[29] Y. Makhlin, G. Schön, and A. Shnirman, Rev. Mod. Phys. **73**, 357 (2001).
[30] G. Wendin and V. Shumeiko, in *Handbook of Theoretical and Computational Nanotechnology*, edited by M. Rieth and W. Schommers (American Scientific Publishers, Valencia, CA, 2006), Ch. 12, e-print arXiv:cond-mat/0508729.
[31] H. J. Lipkin, N. Meshkov, and A. J. Glick, Nucl. Phys. **62**, 188 (1965).
[32] R. Botet and R. Jullien, Phys. Rev. B **28**, 3955 (1983).
[33] A. Messiah, Quantum Mechanics, Vol. 2 (North-Holland, Amsterdam, 1962).
[34] S. Sachdev, *Quantum Phase Transition* (Cambridge University Press, Cambridge, 1999).
[35] W. H. Zurek, U. Dorner, and P. Zoller, Phys. Rev. Lett. **95**, 105701 (2005).
[36] A. Polkovnikov and V. Gritsev, Nature Physics **4**, 477 (2008).
[37] F. Pellegrini, S. Montangero, G. E. Santoro, and R. Fazio, Phys. Rev. B **77**, 140404(R) (2008).
[38] S. Deng, G. Ortiz, and L. Viola, Europhys. Lett. **84**, 67008 (2008).
[39] C. De Grandi and A. Polkovnikov, in *Quantum Quenching, Annealing and Computation*, edited by A. Das, A. Chandra, and B. K. Chakrabarti, Lect. Notes in Phys., Vol. 802 (Springer, Heidelberg, 2010).
[40] U. Divakaran, V. Mukherjee, A. Dutta, and D. Sen, in Quantum Quenching, Annealing and Computation, edited by A. Das, A. Chandra, and B. K. Chakrabarti, Lect. Notes in Phys., Springer, Heidelberg (2009, to be published), e-print arXiv:0908.4004.
[41] J. Dziarmaga, Adv. Phys. **59**, 1063 (2010).
[42] A. Polkovnikov, K. Sengupta, A. Silva, and M. Vengalattore (2010), e-print arXiv:1007.5331.
[43] T. Caneva, R. Fazio, and G. E. Santoro, Phys. Rev. B **78**, 104426 (2008).
[44] V. Giovannetti, S. Lloyd, and L. Maccone, Phys. Rev. A **67**, 052109 (2003).
[45] M. Murphy, S. Montangero, V. Giovannetti, and T. Calarco, Phys. Rev. A **82**, 022318 (2010).
[46] V. Balachandran and J. Gong, Phys. Rev. A **77**, 012303 (2008).
[47] X. Wang, A. Bayat, S. G. Schirmer, and S. Bose, Phys. Rev. A **81**, 032312 (2010).
[48] F. Platzer, F. Mintert, and A. Buchleitner, Phys. Rev. Lett. **105**, 020501 (2010).
[49] J. I. Latorre, R. Orus, E. Rico, and J. Vidal, Phys. Rev. A **71**, 064101 (2005).
[50] P. Calabrese and J. Cardy, J. Stat. Mech. (2005) P04010.
[51] W. Dur, L. Hartmann, M. Hein, M. Lewenstein, and H.-J. Briegel, Phys. Rev. Lett. **94**, 097203 (2005).
[52] J. I. Latorre and A. Riera, J. Phys. A: Math. Theor. **42**, 504002 (2009).
[53] C. Zener, Proc. R. Soc. A **137**, 696 (1932).
[54] F. Caruso, S. Montangero, T. Calarco, S. F. Huelga, and M. B. Plenio, e-print arXiv:1103.0929.